AIP Advances

CHF enhancement partitioning based on surface wettability and porosity on CeO_2 nanoparticle coated surface

Cite as: AIP Advances **9**, 095040 (2019); https://doi.org/10.1063/1.5121918
Submitted: 29 July 2019 . Accepted: 09 September 2019 . Published Online: 24 September 2019

J. Y. Kim, and I. C. Bang

CHF enhancement partitioning based on surface wettability and porosity on CeO_2 nanoparticle coated surface

Cite as: AIP Advances 9, 095040 (2019); doi: 10.1063/1.5121918
Submitted: 29 July 2019 • Accepted: 9 September 2019 •
Published Online: 24 September 2019

J. Y. Kim and I. C. Bang[a]

AFFILIATIONS

Department of Nuclear Engineering, Ulsan National Institute of Science and Technology (UNIST), 50 UNIST-gil, Ulju-gun, Ulsan 44919, South Korea

[a]Author to whom correspondence should be addressed; electronic mail: icbang@unist.ac.kr

ABSTRACT

The experimental boiling critical heat flux (CHF) behavior of CeO_2 nanoparticles coated surface under various deposition condition was experimentally measured. The CHF behavior of CeO_2 nanoparticles coated surface was analyzed based on coupled analysis of surface wettability and capillarity. The surface conditions were modulated by changing the volume concentration and deposition time during the nanoparticles coating process. The convex shaped CHF behavior was observed along with the volume concentration of nanofluid. The analysis based on a single parameter such as surface wettability and capillarity couldn't explain the complex CHF behavior. The novel way to explain the complex CHF behaviors of CeO_2 nanoparticles coated surface is proposed. The model in this study considered the coupling behavior of surface rewetting and liquid transport by capillary wicking motion through the CHF enhancement partitioning. This efforts for the coupling of different physical phenomena on the boiling crisis condition will be beneficial to precise prediction of boiling CHF values on the engineered heater surface.

I. INTRODUCTION

The enhancement of boiling CHF can improve the economics and safety of heat flux-controlled system by allowing the operation with increased power density. There have been extensive research efforts to enhance the boiling CHF through surface modification for decades. The pool boiling experiment on 3-D structure embedded surface shows enhanced CHF performances from previous studies and suggests that reason for CHF enhancement is attributed to enhanced the surface wettability,[1,2] formation of the porous structure,[3,4] and modification of material thermal properties.[5–8]

One of the proposed techniques for surface modification is depositing the nanoparticles on the heater surface by utilizing the nanofluid which is a colloidal suspension of nano-scale particles in the base fluid. The pool boiling experiment conducted by previous researchers with various kind of nanofluids shows significantly enhanced CHF results. Kim et al.,[1] perform the wire pool boiling experiment with SiO_2, ZrO_2, Al_2O_3 and suggest that the significant surface wettability change due to deposition of metal oxide nanoparticles is a key parameter of nanofluid CHF enhancement. Kim et al.[4] found the dependence of nanofluid CHF with capillary wicking length. They show the role of capillary wicking on additional liquid flow on nanoparticles deposited surface. The wire boiling experimental result with graphene and graphene oxide by Park et al.[5] shows the effect of material thermal properties on CHF. The enhanced CHF of graphene oxide nanosheet deposited surface was observed by effective heat dissipation on the local dry spot due to increased thermal activity.

The previous pool boiling CHF researches with nanoparticle deposited surface are mainly focused on the trend analysis based on single enhancement parameters. However, this method has a clear limitation on the precise prediction of CHF for nanoparticles deposited surface. The boiling crisis involves the complex coupled physical phenomena such as surface re-wetting and capillary pumping in the porous layer and heat conduction inside the heater material simultaneously.[9] Therefore, precise pool boiling CHF prediction

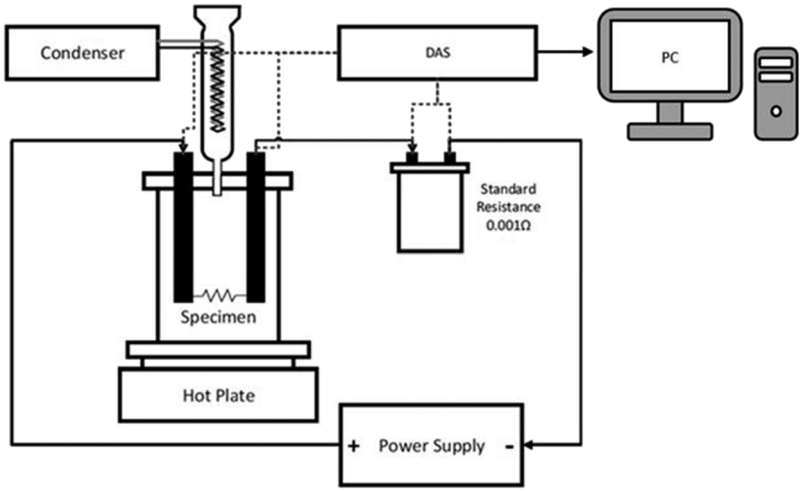

FIG. 1. The schematic configuration of experimental apparatus in this study.

requires the coupled analysis of the different physical phenomenon. The quantitative analysis of coupled phenomena on nanoparticle deposited surface CHF was very limited and was not fully understood. In this paper, we provide a physically coupled CHF prediction analysis result on nanoparticle deposited surface based on the effect of surface wettability and capillarity.

II. EXPERIMENTAL SETUP

The saturated wire pool boiling experiment under atmospheric condition was performed. The schematics of the experimental apparatus are depicted in Figure 1. The Pyrex glass basin (10cm x 5cm x 12cm) was used as pool. The hot plat was utilized to keep the working fluid temperature up to saturation temperature. The reflex condenser located upper side of the Pyrex glass pool to maintain the volume concentration of working fluid during the experiment. The NiCr (20/80) wire with 0.5mm diameter and 55.0mm length was used as a heater. The Teflon block was located upper side of the glass pool to seal the test apparatus. The two copper rods which connected to Teflon block lead the electrical current into the NiCr wire. All the data was recorded by the data acquisition system (Agilent 34980A). The 5.25kW DC power supply (150V, 35A) was utilized to modulate the power level by Joule heating method during the experiment.

The deposition of CeO_2 nanoparticles (d<25 nm) through boiling of nanofluid is used to modify the surface condition. The CeO_2 nanoparticles coated NiCr specimens under designated coating condition are made before the measurement of CHF to prevent the transient deposition of nanoparticles on the heater surface during experiment.[10] The procedures for the nanoparticles coating are depicted in Figure 2. It is known that nanoparticles deposition condition on the heater surface during the boiling is affected by various conditions (applied heat flux, applied boiling deposition time, and volume concentration of nanofluid). The CeO_2 nanoparticles coated surface conditions were modified by modulating the volume concentration (0.0001, 0.001, 0.01, 0.1 vol.%) and deposition time (20, 40 min). The applied heat flux during the nanoparticles coating process is kept constant as 600 kW/m^2. After the coating with CeO2 nanoparticles on the heater surface, pre-deposited specimens are immersed in pure DI water for measurement of CHF.

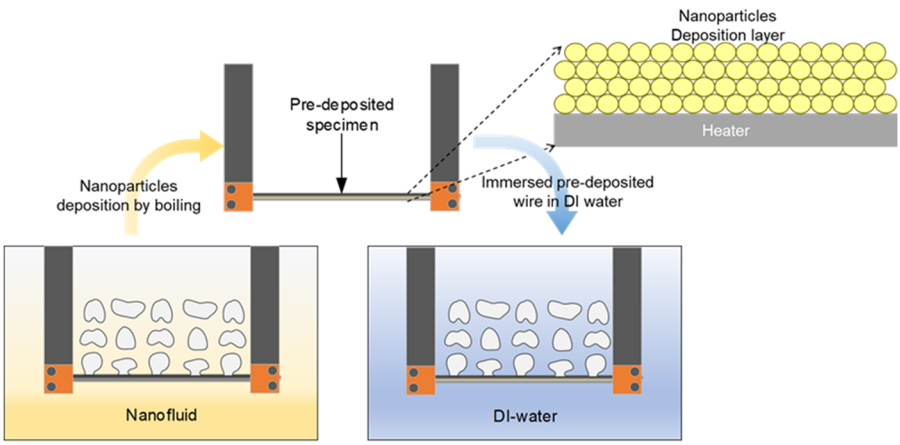

FIG. 2. The procedure for the nanoparticles coating on the bare NiCr wire before the measurement of CHF.

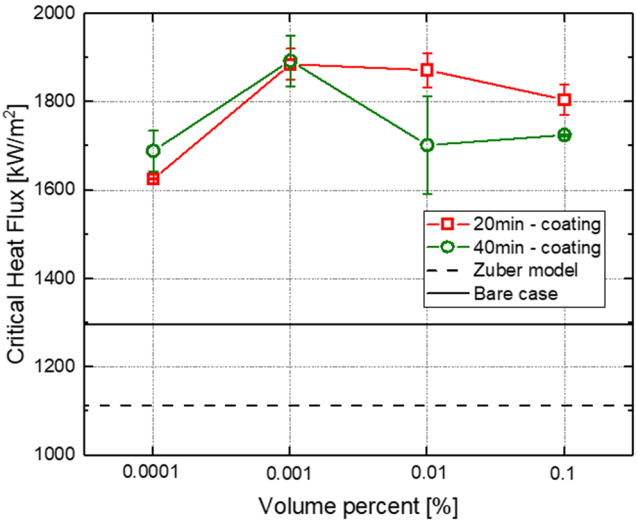

FIG. 3. Critical heat flux measurement results for CeO_2 coated surface under various deposition condition.

The CeO_2 shows similar thermal conductivity and thermal diffusivity with UO_2 (Uranium dioxide) below the temperature of 1,000 K.[11–13] The UO_2 is widely used in the nuclear power plant as a fuel. One can expect that studying the CHF behavior of CeO_2 nanoparticle coated surface can provide the physical insight into the usage of nanoparticle form of UO_2 nuclear fuel in nuclear power plants from the view point of thermal margin (CHF).

III. RESULT AND DISCUSSION

The averaged CHF value for bare NiCr wire was 1,145 kW/m^2 with a 2.87% deviation with Zuber prediction model[14] (1,113 kW/m^2) based on hydrodynamic instability theory. The deposition of CeO2 nanoparticles was confirmed by the scanning electron microscope (SEM) which is discussed in later section. The experimental CHF values for CeO_2 coated surface under various deposition condition are depicted in Figure 3. The changing the deposition time from 20min to 40min did not show a big difference on the CeO_2 nanoparticles coated surface except for the case of 0.01vol.% case. The maximum CHF enhancement of 45.87% was observed for 40min-0.001vol.% deposition condition. The increase of volume concentration of nanofluid from 0.0001 to 0.01vol.% cause increase of CHF for both deposition time condition. However, the reduction of CHF enhancement was observed the volume concentration between 0.01 and 0.1vol.%. This convex shaped CHF behavior of CeO_2 nanoparticles coated surface along the increasing volume concentration was analyzed based on surface wettability and capillarity change based on nanoparticles deposited surface condition.

A. Surface morphology change due to nanoparticles coating

The SEM images nanoparticles coated surface for each deposition condition can be found in Figure 4. The increasing of volume concentration of nanofluid and deposition time during nanoparticles coating process results more densely packed deposition structures on the NiCr wire and more aggregation of nanoparticles. However, further, increase of volume concentration from 0.01 to 0.1 vol.% cause the chaotic and irregular deposition patterns as shown in Figure 4. For the case of least volume concentration case (0.0001 vol.%), the NiCr wire is not fully cover by CeO_2 nanoparticles due to the thin thickness of the layer.

The nanoparticles deposition thickness and surface morphology were confirmed by the three-dimensional (3-D) scanning. Figure 5 shows the vertical height variation on bare NiCr due to nanoparticles deposited layer wire surface. As shown in Figure S3, bare NiCr surface shows almost flat geometry compared to nanoparticles coated surfaces. The increase of CeO_2 nanofluid volume concentration during the coating process causes the thicker nanoparticles coated layer on the NiCr surface. Also, as mentioned above, the CeO_2 coating case with least CeO_2 nanofluid volume concentration

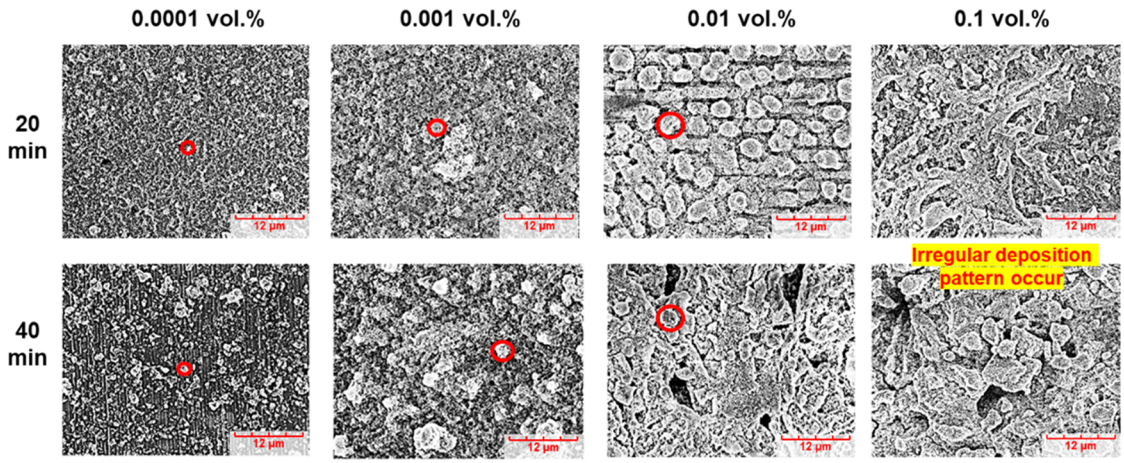

FIG. 4. The procedure for the nanoparticles coating on the bare NiCr wire before the measurement of CHF.

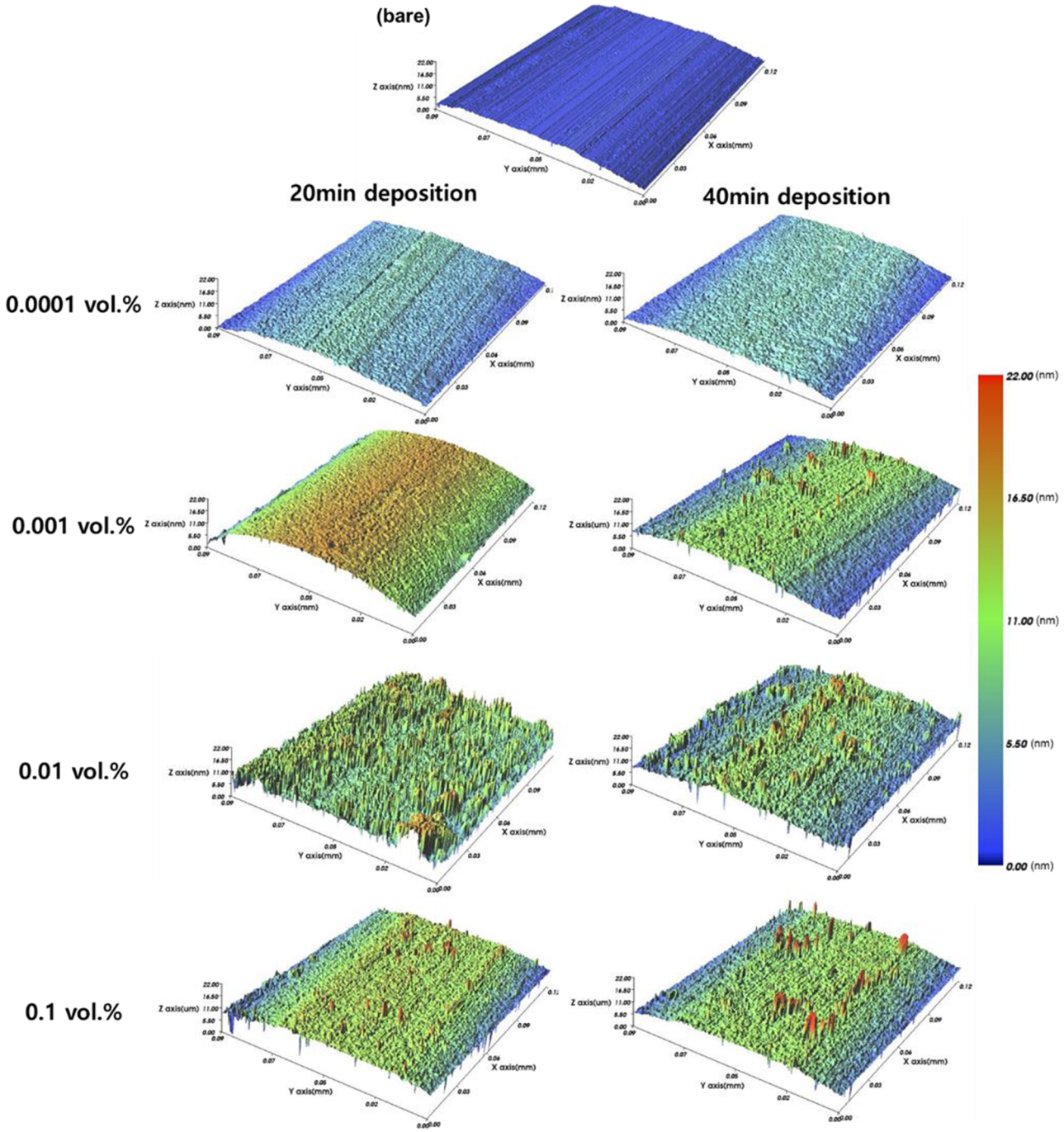

FIG. 5. Three-dimensional scanning analysis results for the CeO_2 nanoparticles coated surface under various coating conditions.

(0.0001vol.%) shows a relatively thin deposition layer compared to the higher volume concentration cases.

B. Effect of surface wettability

The effect of surface wettability on nanoparticle deposited surface CHF was analyzed based on measured static contact angle. The Kandlikar[2] model based on the force balance was utilized to analyze the surface wettability change effect due to deposition of nanoparticles on the heater surface. The comparison result is shown in Figure 6. The significant reduction of static contact angle on CeO_2 nanoparticles coated surface was observed. The corresponding CHF values show enhanced CHF due to increased surface wettability.

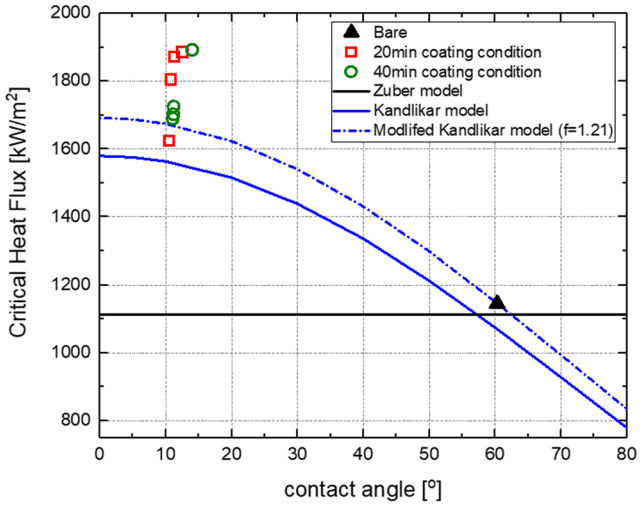

FIG. 6. Comparison of effect of surface wettability change on boiling CHF based on modified Kandlikar model (*f=1.07*) with static contact angles (~11.56°).

The correction factor (f=1.07) was multiplied to original Kandlikar model[15] to compensate for the deviation between bare NiCr CHF as depicted in equation (1).

$$q''_{Modified\ Kandlikar} = f \times h_{fg}\rho_g^{1/2}\left(\frac{1+\cos\beta}{16}\right)\left[\frac{2}{\pi}+\frac{\pi}{4}(1+\cos\beta)\cos\phi\right]^{1/2} \times [\sigma g(\rho_l-\rho_g)]^{1/4} \quad (1)$$

Where h_{fg} is latent heat of phase change, ρ_g is density of gaseous phase, β is measured contact angle, ϕ is orientation angle, σ is surface tension, g is gravitational acceleration and ρ_l is density of liquid phase respectively. The smallest volume concentration cases (0.0001vol.%) for both deposition time shows good agreement with modified Kandlikar model with the maximum deviation of 2.78%. We assume that CHF enhancement of 0.0001vol.% case is due to purely wettability effect and averaged static contact angle of ~11.56° for CeO_2 nanoparticles coated surface is representative static contact angle of nanoparticles coated surface. However, the vertical dispersion of CHF data for nanoparticles coated surface was observed at the static contact angle of ~11.56°. This result indicates that surface wettability effect alone can't explain the CHF enhancement behavior for nanoparticles coated surface. Based on the previous researches results,[4,15,16] formation of capillarity inside the nanoparticle deposited layer was pointed out as the main reason for the vertical dispersion of CHF data in Figure 6. Therefore, the form of CHF partitioning model is assumed as a linear summation of modified Kandlikar model and CHF enhancement term from capillarity as depicted in equation (2). Where $\langle u_{l,p}\rangle$ is the liquid flow rate inside the porous nanoparticles coated layer by capillary motion.

$$q''_{CHF} = f \times h_{fg}\rho_g^{1/2}\left(\frac{1+\cos\beta}{16}\right)\left[\frac{2}{\pi}+\frac{\pi}{4}(1+\cos\beta)\cos\phi\right]^{1/2} \times [\sigma g(\rho_l-\rho_g)]^{1/4} + \rho_l\langle u_{l,p}\rangle h_{fg} \quad (2)$$

C. Effect of surface capillarity

The porosity is the most important parameter determining the ability of capillarity inside the porous media. The porosity values for nanoparticles deposited surface are measured by pixel counting method and detailed process are depicted in supplementary material. The resulted porosity values are plotted in Figure 7(a). The increase of CeO_2 nanofluid volume concentration up to 0.01vol.% cause decrease of porosity during the coating process. However, the increased porosity of coated surface was observed for the volume concentration between 0.01 and 0.1vol.%. The increased porosity can be attributed to the irregular chaotic nanoparticles deposition pattern which can be found in Figure 4.

Measuring the capillary wicking length defined by Jurin's law is a representative and most widely used method of indirectly measuring the capillarity of porous media. The comparison between measured capillary wicking height and CHF enhancement was made and shown in Figure 7(b). The comparison results show an inconsistent trend between measured capillary wicking length and CHF enhancement ratio. The maximum wicking height condition (0.01 vol.%) didn't match with the maximum CHF condition (0.001 vol.%).

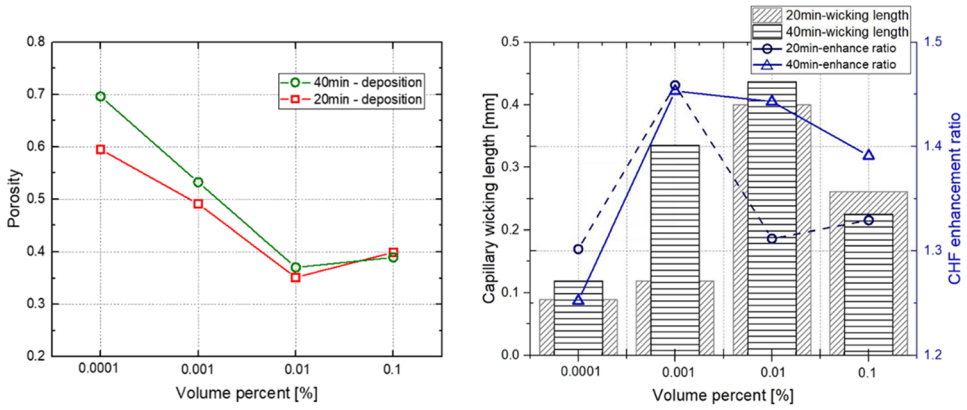

FIG. 7. The calculated porosity values for different deposition conditions (a) and comparison result with measured capillary wicking height and prediction value based on Jurin's model (b).

The reason for this inconsistency can be found from the definition of capillary wicking height followed by Jurin's law. This law assumes the static condition of working fluid inside the porous layer and do not consider the dynamic viscous drag inside it. However, in actual boiling condition, working fluid is transported inside the porous layer and the effect of viscous drag cannot be neglected.

IV. MODELING OF LIQUID TRANSPORTATION INSIDE NANOPARTICLES COATING LAYER

To reflect the effect of viscous drag in modeling of CHF on nanoparticles deposited surface, capillary driven liquid flow rate was modeled. The capillary pumping liquid flow rate ($\langle u_{l,p} \rangle$) inside the porous layer was modeled by balancing the capillary pressure and viscous drag pressure drop. The assumption was made that only the liquid phase is transported inside the porous media since the thickness of the nanoparticles coated layer is the order of micron or less. The viscous pressure drop inside the porous layer was governed by Darcy-Ergun momentum relation which is depicted in equation (3).

$$\Delta P_l = \rho_l g \sin\Omega - \frac{\mu_l}{K}\langle u_{l,p} \rangle - \frac{C_E}{K^{1/2}}\rho_l |\langle u_{l,p} \rangle| \langle u_{l,p} \rangle \tag{3}$$

$$K = \frac{\varepsilon^3 d^2}{180(1-\varepsilon)^2} \tag{4}$$

$$C_E = \left(\frac{0.018}{\varepsilon^3}\right)^{1/2} \tag{5}$$

$$P_{c,Max} = C_J \frac{\sigma}{(K/\varepsilon)^{1/2}} \tag{6}$$

Where the ΔP_l is liquid phase pressure drop inside the porous layer, Ω is orientation angle, μ_l is viscosity of working liquid, K is permeability of porous media, C_E is correction coefficient for Stoke's flow, $\langle u_{l,p} \rangle$ is volume averaged liquid flow rate inside the porous media, ε is porosity of porous media, d is pore diameter, and σ is surface tension. The permeability (K) and Stoke's flow coefficient (C_E) were modeled followed by Carmen-Kozeny model. The pore diameter in equation (4) is assumed to be same with CeO_2 nanoparticles diameter (~25nm) to simplify the calculation. The maximum capillary pressure inside the porous media was modeled by Leverett-J function.

The comparison was made between measured capillary wicking length and predicted one was made to determine the C_J values in equation (6). The capillary wicking length defined by Jurin's law is depicted in equation (7). Where $h_{wicking}$ is capillary wicking length, P_c is capillary pressure, ρ_l is density of the liquid, g is gravitational acceleration constant, and Ω (90°) is orientation angle. The capillary wicking height was measured at room temperature condition (25°C) with DI water. Therefore, the corresponding liquid density at 25°C (997.16 kg/m^3) was used in modeling of capillary wicking length. The capillary pressure (P_c) inside the equation (7) is replaced with maximum capillary pressure modeled by Leverett-J function which is depicted in equation (6). The final form of capillary wicking length in this study is given as a function of porosity as shown in equation (8). The comparison results of the prediction model and actual capillary length are present in Figure 8.

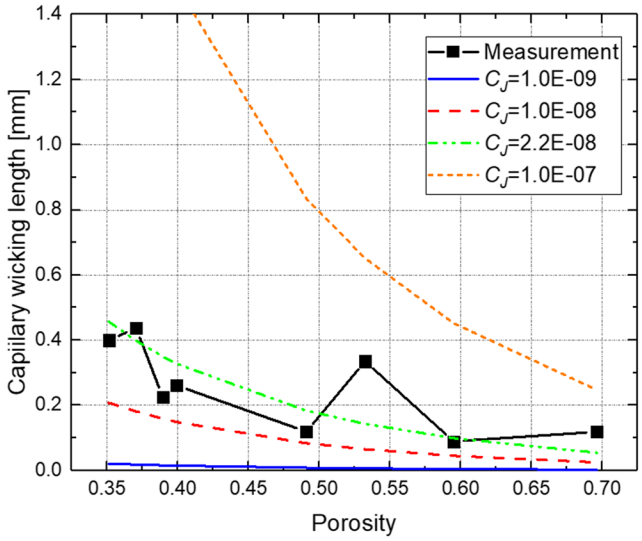

FIG. 8. The comparison results with measured capillary wicking height and predicted capillary wicking height based on proposed model.

The C_J value was varied from 1.0E-07 to 1.0E-09. The increase of C_J value in prediction model results in larger capillary wicking length value due to increased capillary pressure inside the prediction model. The value of 2.2E-08 shows good agreement between the prediction model and measured capillary wicking length with a maximum deviation of 57.20%. Therefore, the C_J value was determined as 2.2E-08 in further study in this paper.

$$h_{wicking} = \frac{P_c}{\rho_l g \sin(\Omega)} \tag{7}$$

$$h_{wicking} = \frac{C_J \sigma}{(K/\varepsilon)^{1/2}\rho_l g \sin(\Omega)} = f(\varepsilon) \tag{8}$$

The used values show a big difference between previous research conducted by Liter and Kaviany[3] (C_J=0.53), Yang and Cheung[17] (C_J=0.48). The previous pool boiling research conducted by Seo et al.[8] with porous graphene and SiC nanoparticles deposited surface report that the proposed liquid transport theory inside has a limitation on the application for nano-scale structure. The result from the previous study guarantees the reliability of the used coefficients for nanoparticles deposited surface.

$$C_J \frac{\sigma}{(K/\varepsilon)^{1/2} l_t} = \frac{\mu_l}{K}\langle u_{l,p} \rangle + \frac{C_E}{K^{1/2}}\rho_l \langle u_{l,p} \rangle^2 \tag{9}$$

The liquid flow rate across the porous nanoparticle deposition layer was calculated by balancing the maximum capillary pressure and maximum pressure drop as depicted in equation (9). Where l_t is characteristics liquid transport length which represent the distance traveled by the liquid inside the nanoparticles coated layer due to capillary pumping pressure. The liquid flow rate ($\langle u_{l,p} \rangle$) inside the nanoparticles coated layer is given as a function of porosity.

The characteristic liquid transport length (l_t) in equation (9) was determined by comparing the experimental CHF with CHF

partitioning model presented in this paper. The characteristic liquid transport length was modulated from 0.05mm to 1.00mm as depicted in Figure 9. Increasing the characteristics transport length in CHF partitioning model results in lower estimation of CHF. The decreased liquid flow rate inside the porous CeO_2 nanoparticles coated surface was observed due to the enhanced viscous pressure drop across the porous media. The value of 0.14mm of characteristics liquid transport length shows good agreement with experimentally measure CHF values on CeO2 nanoparticles coated surface under various deposition condition with a maximum error of 3.52%. Therefore, the characteristics transport length of 0.14mm is selected as utilized in this CHF partitioning modeling process.

The CHF partitioning results are calculated as depicted in equation (2) with calculated liquid flow rate and static contact angle (~11.56°). Since the CHF enhancement for 0.0001vol.% coating condition was attributed to purely wettability effect as mentioned earlier. The effect of the capillary was not considered in this case, since the nanoparticles coated layer thickness is very thin compared to the other coating conditions and the surface is not fully covered with nanoparticles as depicted in Figure 4–5. The comparison result is shown in Figure 10. The maximum deviation between prediction values and experimental values are 3.52%.

The early mentioned inconsistency problem between CHF trend with measured parameters such as static contact angle and capillary wicking height can be explained by adopting this partitioning approach. At surface porosity between 0.60 and 0.50, capillary pressure is formed inside the nanoparticles coated layer and its effect dominate the liquid transport. Therefore, in this porosity region, decrease of porosity cause increase of CHF. However, further decrease of porosity cause more rapid drop of permeability inside the porous layer and the effect of viscous drop becomes dominant and the corresponding liquid flow rate also decreases. The decreased liquid flow rate results in the reduction of CHF in lower porosity region. The CHF enhancement was partitioned into two terms. The first one is CHF enhancement through surface wettability change which acts as a baseline for CHF enhancement behaviors, and the other one is enhancement through additional liquid supply due to capillary pumping inside the porous layer. The latter one is responsible for the vertical CHF variation on the contribution of surface wettability.

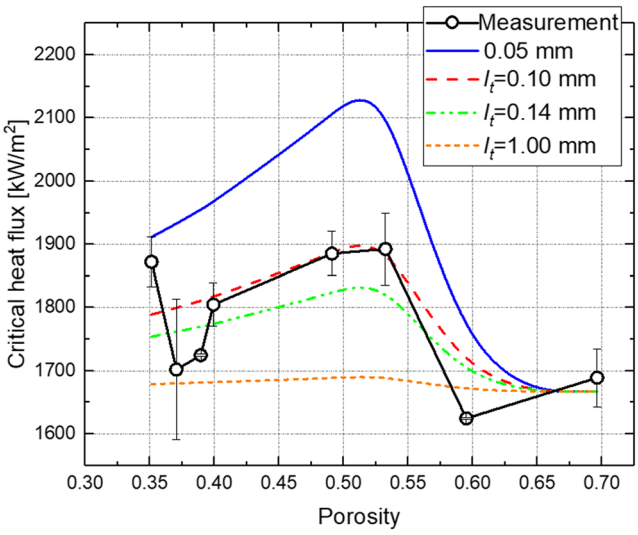

FIG. 9. The comparison results of measured critical heat flux values and predicted CHF values based on the proposed critical heat flux partitioning method.

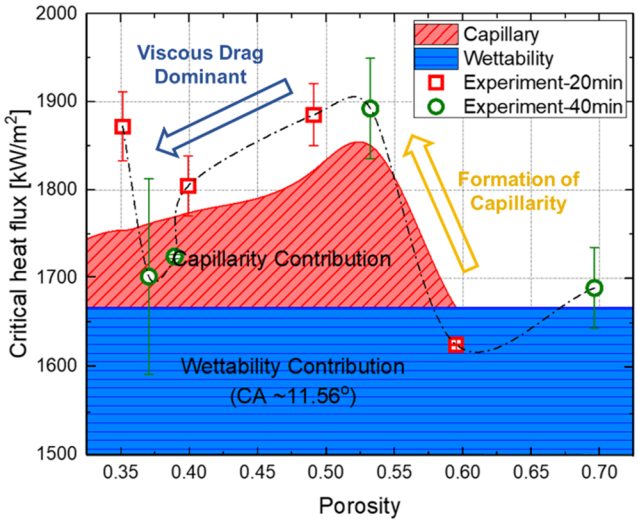

FIG. 10. CHF enhancement partitioning result based on surface wettability and capillarity based on nanoparticles coated surface parameters (static contact angle, porosity of coated layer).

V. CONCLUSION

The present model successively explains the CHF enhancement behavior on nanoparticles coated surface and suggests that the CHF enhancement behavior on the nanoparticles coated surface can be partitioned by the effects of surface wettability and capillarity. The key parameters in determining the CHF enhancement behavior are the static contact angle and the porosity of the nanoparticles coated layer. The analysis result in this study indicates that coupling the different physical phenomena (surface rewetting and capillary wicking) is essential for precise prediction of CHF enhancement rather than just comparing with single parameters. Also, the effect of viscous pressure drop of working fluid inside the porous media should be considered in the modeling of CHF values on the porous surface. The coefficients used in modeling of permeability and correction coefficient on Stoke's flow on nano-scale porous media has lots of uncertainty and should be further validated or modified for the precise CHF prediction on nanoparticles coated surface.

SUPPLEMENTARY MATERIAL

See supplementary material for detailed description of experimental procedure, uncertainty analysis, and procedure for measurement of porosity.

ACKNOWLEDGMENTS

This research was supported by Basic Science Research Program through the National Research Foundation of Korea (NRF) funded by the Korea government (MSIT) (No. 2017R1A2B2008031).

REFERENCES

[1]S. J. Kim, I. C. Bang, J. Buongiorno, and L. W. Hu, Int. J. Heat Mass Transf. **50**, 4105 (2007).
[2]S. G. Kandlikar, J. Heat Transfer **123**, 1071 (2001).
[3]S. G. Liter and M. Kaviany, Int. J. Heat Mass Transfer **44**, 4287 (2001).
[4]H. D. Kim and M. H. Kim, Appl. Phys. Lett. **91**, 1 (2007).
[5]S. D. Park, S. Won Lee, S. Kang, I. C. Bang, J. H. Kim, H. S. Shin, D. W. Lee, and D. Won Lee, Appl. Phys. Lett. **97**, 023103 (2010).
[6]H. S. Ahn, J. M. Kim, T. Kim, S. C. Park, J. M. Kim, Y. Park, D. I. Yu, K. W. Hwang, H. Jo, H. S. Park, H. Kim, and M. H. Kim, Sci. Rep. **4**, 6276 (2014).
[7]H. Seo, H. D. Yun, S. Y. Kwon, and I. C. Bang, Nano Lett. **16**, 932 (2016).
[8]H. Seo, J. H. Chu, S. Y. Kwon, and I. C. Bang, Int. J. Heat Mass Transf. **82**, 490 (2015).
[9]J. Buongiorno, Ann. Nucl. Energy **63**, 9 (2014).
[10]S. M. Kwark, R. Kumar, G. Moreno, J. Yoo, and S. M. You, Int. J. Heat Mass Transf. **53**, 972 (2010).
[11]A. T. Nelson, D. R. Rittman, J. T. White, J. T. Dunwoody, M. Kato, and K. J. McClellan, J. Am. Ceram. Soc. **97**, 3652 (2014).
[12]C. Ronchi, M. Sheindlin, M. Musella, and G. J. Hyland, J. Appl. Phys. **85**, 776 (1999).
[13]J. K. Fink, J. Nucl. Mater. **279**, 1 (2000).
[14]N. Zuber, United States At. Energy Commision 196 (1959).
[15]H. S. Ahn, C. Lee, J. Kim, and M. H. Kim, Int. J. Heat Mass Transf. **55**, 89 (2012).
[16]N. S. Dhillon, J. Buongiorno, and K. K. Varanasi, Nat. Commun. **6**, 8247 (2015).
[17]J. Yang and F. B. Cheung, Int. J. Heat Fluid Flow **26**, 474 (2005).